J. Fluid Mech. (1995), *vol.* 293, *pp.* 81–98

Experimental study of convection in a mushy layer during directional solidification

By C. F. CHEN

Department of Aerospace and Mechanical Engineering, The University of Arizona, Tucson, AZ 85721, USA

(Received 4 March 1994 and in revised form 6 January 1995)

Results of experiments using a number of techniques to study the nature of convection in a mushy layer generated by directional solidification of aqueous ammonium chloride solutions are reported. The techniques include flow visualization using a dye tracing method to study convection within the mushy layer before and after the onset of plume convection, and X-ray tomography to measure the solid fraction of a growing mush. The principal results are as follows. (i) Prior to the onset of chimneys, there is no convective motion in the mush, in spite of the vigorous finger convection at the mush–liquid interface. (ii) When the plume convection is fully developed, the flow of fluid in the mush consists of a nearly uniform downward motion toward the bottom of the tank, horizontal motion along the bottom toward the chimneys, then upward plume motion through the chimneys in the liquid region above the mush. (iii) The solid fraction of a growing mush as determined by X-ray tomography shows a significant decrease toward the bottom of the tank after the chimneys are fully developed. As a result, the concomitant increase in the local permeability can be as much as 50%. Some of the results reported herein confirm theoretical predictions of Worster (1992) and Amberg & Homsey (1993). Others reveal phenomena not observed heretofore.

1. Introduction

Alloy castings made by directional solidification, a process in which the melt is solidified by cooling from below, exhibit increased resistance to creep rupture and improved thermal fatigue behaviour. Defects in the form of freckles, however, may occur, concentrating the lighter solute in longitudinal columns in the casting and have a detrimental effect on the strength of the finished product. It was established by the experiments of McDonald & Hunt (1970) and Copley *et al.* (1970) using aqueous ammonium chloride solution, an analogue system for binary metallic alloys, that the origin of the freckles can be traced to the plume convection in the mushy layer. Sample & Hellawell (1984), using liquid nitrogen as coolant, as was done by the previous investigators, were able to induce the onset of plumes, with their associated chimneys, by withdrawing fluid near the mush–liquid interface through a small pipette at the time when plume convection first appeared. Based on these experimental results, Hellawell (1987) and Hellawell, Serazin & Steube (1993) conjectured that the onset of plume convection is caused by finite-amplitude disturbances in the boundary layer at the mush–liquid interface. Chen & Chen (1991), Tait & Jaupart (1992*a*), Tait, Jahrling & Jaupart (1992), and Chen, Lu & Yang (1994) conducted experiments using coolant from constant-temperature baths to effect a much smaller cooling rate. This enabled them to examine the sequence of events in more detail and to determine the critical

conditions in the mushy layer for the onset of plume convection. It is their opinion that the onset of plume convection is due to instabilities in the mushy layer. This idea is reinforced by the linear stability theory of Worster (1992) and by the weakly nonlinear analysis of Amberg & Homsy (1993).

In the initial stages of the solidification process, there is rapid crystallization at the bottom of the tank, releasing cooler but less concentrated fluid, which induces salt-finger convection just above the mush–liquid interface. As the mush grows thicker, the critical condition in the mush is exceeded, then chimneys start to appear in the mush, and plumes of much lighter fluid flow upward through the chimneys into the liquid and then rise to much greater heights than the salt-finger cells. When finally solidified, the lighter element, water in this case, is concentrated by these chimneys into discrete vertical cylinders, the counterpart of freckles in metallic alloys (see Sarazin & Hellawell 1988).

Worster (1992) considered the linear stability of the combined liquid and mush regions during directional solidification, taking into account the interaction between buoyancy-driven convection and the melting–solidification process in the mush. His results show that there are two distinct modes of instability: one is the boundary layer mode occurring at the mush–liquid interface with convection cells of small wavelengths, and the other is the mushy-layer mode with wavelengths comparable to the thickness of the layer. There is hardly any coupling between these two modes. Under a number of plausible conditions, the mushy-layer mode of instability can be the critical one, but typically the boundary-layer mode sets in much earlier. The thermodynamic property of the system promotes local melting in the upwelling region and enhanced solidification in the downflow region. This process eventually leads to the formation of chimneys, as shown by Amberg & Homsy (1993) through a weakly nonlinear analysis. Their results also show that onset of plume convection is a subcritical instability initiated by a finite-amplitude perturbation. Chen *et al.* (1994) solved the linear stability equations of Worster (1992) numerically and obtained results over a range of parameters. They found that, for parameters typical of the experimental conditions for NH_4Cl solutions, the boundary-layer mode is the dominant unstable mode.

In this paper, we report the results of experiments designed to gain a better knowledge of the convection process in the mush. The first set is carried out in a three-dimensional tank using a dye tracing method to examine convection in the mush before and after the onset of plume convection. The second set is carried out in a Hele–Shaw cell so that convection occurs in a two-dimensional geometry. This apparatus also has the added advantage of offering a much clearer view of the solidification process and the flow in the chimneys, since they are transparent. In the third set, the growing mush is repeatedly scanning using X-ray tomography so that the three-dimensional distribution of solid fraction within the mush can be determined. The last set examines the possibility of generating chimneys with plume convection by suction when the cooling rate is lower than that provided by liquid nitrogen. These experiments and their results are discussed in turn in the following sections.

2. Dye tracing experiments

All dye tracing experiments were carried out in a tank $19.5 \times 15 \times 30$ cm tall with Plexiglas sides and a copper bottom. A solution of 26% NH_4Cl–H_2O was directionally solidified by maintaining the bottom at -9 °C using a constant-temperature bath. The temperature of the coolant was set such that no eutectic layer was formed. Three sets of dye tracing experiments were conducted. The first was for an inactive mush to

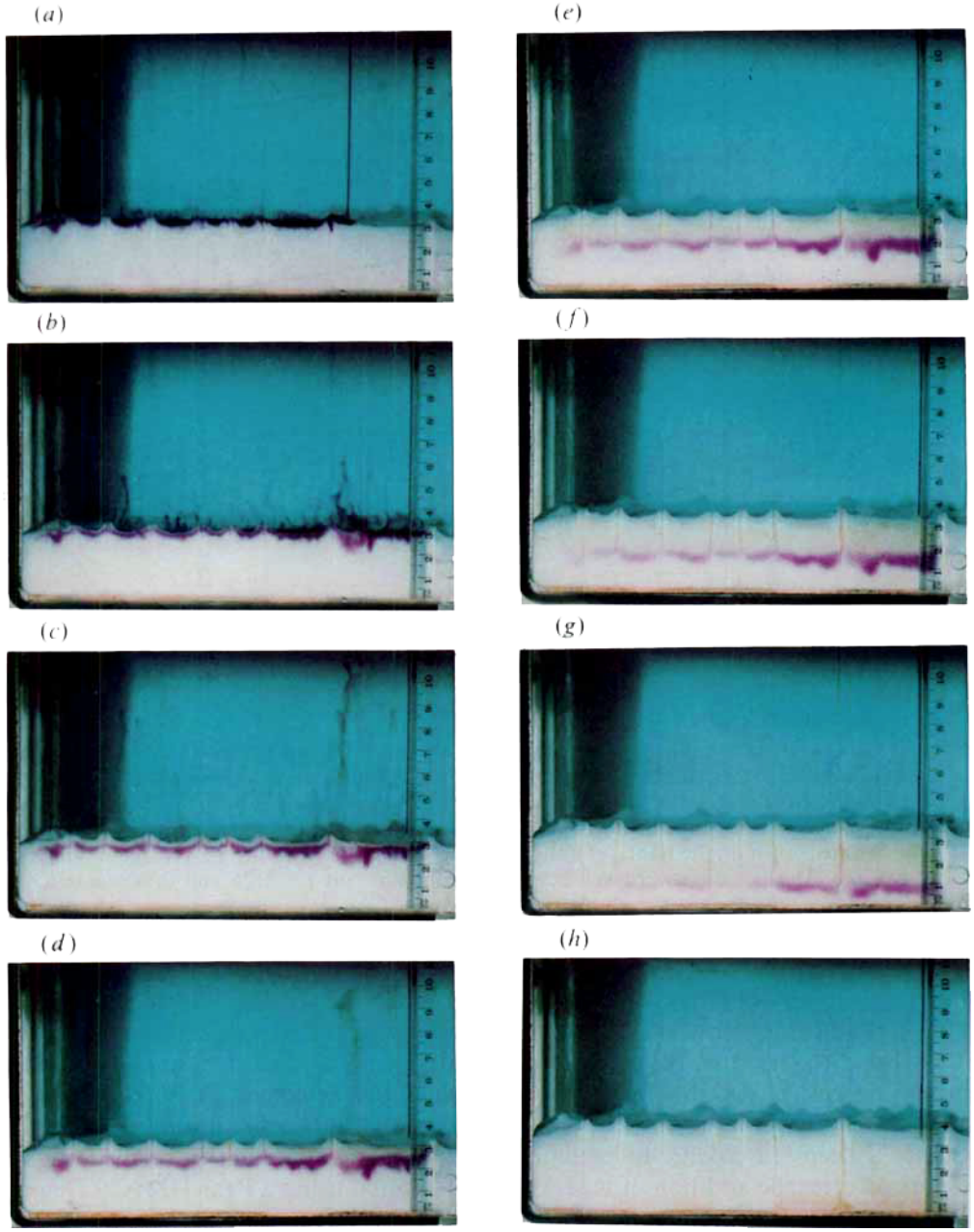

FIGURE 1. Motion of dyed solution through a mushy layer when the plume convection is fully developed. (*a*) $t = 2{:}10$ – input of dyed solution; (*b*) $t = 2{:}12$ – some dyed solution being carried upward by finger convection; (*c*) $t = 2{:}15$ – appearance of billows along the bottom of the dyed line; (*d*) $t = 2{:}20$, (*e*) $t = 2{:}30$, and (*f*) $t = 2{:}40$ – steady downward motion of the dyed line and some withdrawal of fluid into the chimneys by the plumes: (*g*) $t = 3{:}00$ – dyed solution is visible in the plumes issuing out of chimney; (*h*) $t = 4{:}20$ – mush is free of dyed solution.

calibrate the natural sinking rate of the dyed solution, which was slightly heavier than the melt in the mush. The second set was conducted in a growing mush when there was vigorous finger convection at the mush–liquid interface, but prior to the onset of plume convection. The third set was conducted in the same growing mush, but at later times

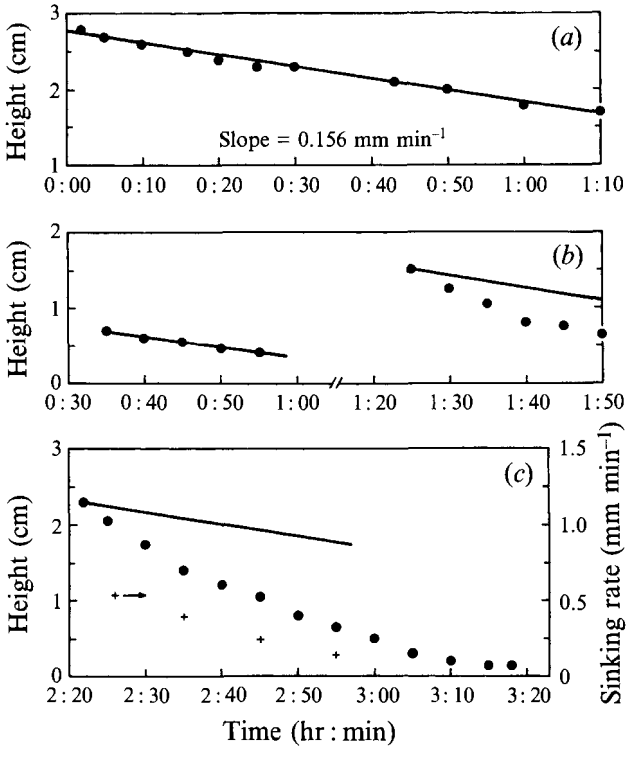

FIGURE 2. Rates of descent of the dyed solution in a mushy layer: ●, vertical position of the dye line. (*a*) Inactive mush: being slightly heavier, the dyed solution has a downward velocity of 0.156 mm min^{-1}. Note that the vertical scale starts at 1 cm. (*b*) Active mush: data obtained prior to the onset of plume convection are shown on the left, and those obtained when the plume convection is developing are shown on the right. (*c*) Fully developed plume convection: +, average sinking rate of the dye line. The net downward velocity is 0.53 mm min^{-1} at $t = 2{:}26$ and 0.14 mm min^{-1} at $t = 2{:}55$.

when plume convection was developing and after it had fully developed. In the following, we describe in some detail the procedure for conducting these experiments.

Just prior to the start of a dye tracing experiment, a small amount of solution, typically 20 ml, is withdrawn from the mush–liquid interface. Into this solution, 0.01–0.02 g of $KMnO_4$ crystals is added. After being thoroughly mixed, the solution assumes a deep-red colour. In preliminary experiments, the density of the solution before and after the addition of $KMnO_4$ was measured using a Paar DMA60 Density Meter. Typically, the density of the solution with dye is increased from 0.05 % to 0.1 %. The dyed solution is then forced by a peristaltic pump through a capillary tube mounted on a traverse mechanism onto the mush–liquid interface. In figure 1, we present a series of photographs showing the motion of the dyed solution in a mush during the fully developed plume convection stage.

Figure 1 (*a*) shows the input of dyed solution along the edge of a transparent wall at $t = 2{:}10$ (2 h, 10 min into the experiment). There are seven chimneys in view, some of their plumes are made visible by the red dye. One minute later, figure 1 (*b*), some of the dyed solution is being carried upward by the finger convection still active at that time, and the rest is being carried into the mush by the general downward fluid motion induced by the upward flux of the plumes. At $t = 2{:}15$, figure 1 (*c*), billows begin to

appear at the lower edge of the dye line due to the Rayleigh–Taylor instability, while the top of the dye line remains parallel to the interface. The photos in figures 1(*d*), 1(*e*) and 1(*f*) were taken 10 min apart, at $t = 2{:}20$, 2:30, and 2:40, respectively. The dye trace moves downward almost uniformly in the spaces between the chimneys. In the neighbourhood of each chimney, dyed solution is being sucked into chimneys and out into the liquid region. In figure 1(*g*), $t = 3{:}00$, the plumes issuing out of the two chimneys on the right are made clearly visible by the dyed solution. By $t = 4{:}20$, the mush is free of dyed solution.

Two different interpretations of the results can be made. One is that the bulk flow in the mushy layer is uniformly downward (except in the neighbourhood of chimneys), horizontal along the bottom, and upward through the chimneys. This interpretation is consistent with the suggestions of Roberts & Loper (1993). Since the descending motion of the dye line is due to the vertical component of the velocity in the mush and any horizontal component of the velocity can only affect the dye intensity, an alternative interpretation is that liquid enters chimneys at all heights, as suggested by Worster (1991). However, it is well known that the solid fraction of the chimney rim is much higher than that of the mush and that an extensive root system exists at the bottom of the chimney. These facts and the recent finding by X-ray tomography that the solids fraction of the mush shows a significant decrease toward the bottom (see §4) indicate that the first interpretation is likely to be the correct one.

It is reasonable to assume that the relative density difference between the dyed and undyed solutions remains constant throughout the experiment in a growing mush, even though the solute concentration of the interstitial fluid is decreasing toward the bottom due to further solidification. This is because, as the dyed solution descends downward, its temperature equilibrates quickly with its surroundings, and its solute concentration is reduced by solidification similar to the undyed solution.

The same type of experiment was conducted in an inactive mush and in an actively growing mush both before and after the onset of plume convection. Quantitative data were obtained by recording the motion of the dye line using a time-lapse motion picture at 1 frame s^{-1}. Data from the inactive mush are shown in figure 2(*a*), with the position of the dye line as a function of time. The straight line obtained by linear regression shows a downward velocity of 0.156 mm min^{-1}.

In the growing mush, the dyed solution was introduced and its motion recorded in three segments. During the first segment, $t = 0{:}35$ to 0:55, there was vigorous finger convection at the mush–liquid interface but no plume convection in the mush. Care was taken to input the dyed solution at suitable rate. At small flow rates, all the dyed solution was carried upward into the liquid region by the vigorous finger convection. At large flow rates, the desired dye line became a dye patch, and no reliable data could be obtained. In this segment, the dye line was essentially horizontal, and the average position of the dye line is shown in the left portion of figure 2(*b*). The straight line through the five data points has the same slope as the line in the inactive mush. It shows that there was no vertical motion of the interstitial fluid during this period, even though vigorous finger convection was occurring at the mush–liquid interface. Since any convective motion in the mushy layer will necessarily have vertical components, the absence of any vertical motion indicates that there was no convective motion present. In the second segment, $t = 1{:}25$ to 1:50, plume convection was developing, and it coexisted with the finger convection. The position of the dye line is shown in the right portion of figure 2(*b*). Again, a straight line with slope = -0.156 mm min^{-1} is drawn through the first data point for comparison. It is seen that the dye line had a net downward velocity, the average value being 0.21 mm min^{-1}.

In the final segment, when the plume convection is fully developed, $t = 2{:}22$ to $2{:}55$, the downward convection became much larger, as shown in figure 2(*c*). The average net downward velocity was found to be 0.53 mm m^{-1} at $t = 2{:}26$ and decreased to 0.14 mm min^{-1} at $t = 2{:}55$ when the dye line was near the bottom of the tank. As indicated in the series of photos shown in figure 1, there was no upward flow through the mush. All upward flow was confined within the chimneys. It is noted that, even at the highest downward velocity, 0.53 mm min^{-1}, it took approximately 100 s for the solution to descend 1 mm. The thermal diffusion time is approximately 7 s for a comparable distance. There is no doubt that the interstitial fluid within the mush was in thermal equilibrium with its surroundings. Results of these experiments confirm the predictions of Worster (1992) based on the linear stability theory that during the period when the boundary-layer mode of instability (finger convection in the experiment) is dominant, there is no motion in the mush. These results also lend support to the assumption of Emms & Fowler (1994) and Worster & Kerr (1994) that the mushy zone can be quiescent while there is vigorous convection in the liquid region.

Sample & Hellawell (1984) were able to induce the onset of plume convection by suction when there was vigorous finger convection in a solidifying NH_4Cl solution cooled from below by liquid nitrogen. I have carried out two such experiments with cooling by a constant-temperature circulator. An extended hypodermic needle with a 60 cm^3 syringe was mounted vertically over the tank to provide suction. At approximately 30 min into the experiment, when the mush was approximately 1 cm thick and chimneys started to appear, the needle was lowered to a level 1–2 mm above the mush surface and 10 cm^3 of fluid were withdrawn in 5–10 s. The needle was then carefully removed from the tank. Within the next 5 min, visual and shadowgraph observations were made at the location where suction was applied. Then another spot on the mush surface was selected, and the procedure repeated. In five attempts no chimney was generated at the locations where suction was applied. The experiment was repeated, with suction started just prior to the onset of chimneys. Out of five attempts, none was successful.

The principal difference between these experiments and those of Sample & Hellawell (1984) is the cooling rate at the bottom. From the temperature distributions in the eutectic given by Chen & Chen (1991) and Hellawell *et al.* (1993), the cooling rate generated by liquid nitrogen is four to five times as large as that generated by a constant-temperature circulator. It may be conjectured that, at large cooling rates with concomitant high freezing rates, the conditions within the mush are not at equilibrium and chimney convection can be generated by the suction process, as well as by instability of the mushy layer. When the cooling rate is much smaller, equilibrium conditions prevail in the mush and finite-amplitude disturbances in the finger convection region are not capable of generating chimneys in the mush. In this case, chimneys can only be generated by the instability mechanism within the mushy layer.

3. Experiments in a Hele-Shaw cell

This set of experiments was designed to provide a clearer view of the onset and subsequent development of finger convection at the mush–liquid interface and the onset and flow through chimneys. In a three-dimensional geometry, the convective motion is occurring in superposed liquid and porous layers. In Hele-Shaw geometry, however, the process is occurring in superposed porous layers of different permeability. It was anticipated that the time scale of the convection process in a Hele-Shaw cell would be larger than that in a three-dimensional tank. This is indeed the case, but most

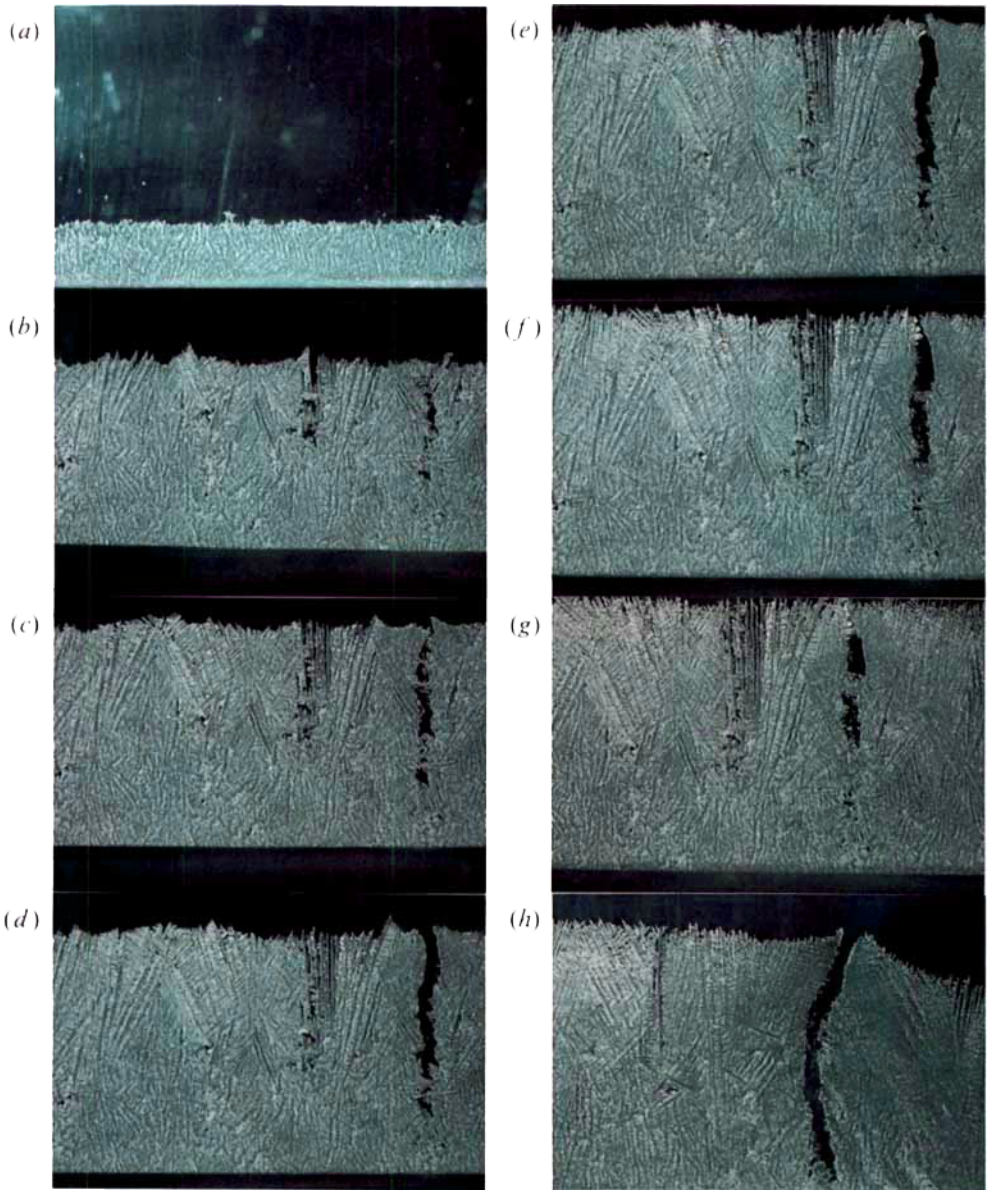

FIGURE 3. Results from a Hele-Shaw cell: close-up of a mushy layer. (*a*) $t = 0{:}15$ – at the start of the solidification experiment, tiny crystals are seen in the convection current; (*b*) $t = 0{:}50$ – two likely sites of chimneys; (*c*) $t = 1{:}05$ and (*d*) $t = 1{:}15$ – development of chimney from the top down; (*e*) $t = 1{:}20$ – exit blocked by crystallization; (*f*) $t = 1{:}30$ and (*g*) $t = 1{:}40$ – slow demise of the chimney; (*h*) $t = 2{:}00$ – there is always lots of activity in an active chimney: tiny crystals are being carried upward by the flow and larger chunks of crystals, loosened by melting, are dropping to the bottom, some of which are caught at the rim of the chimney.

other aspects, such as the initial finger convection giving way to the development of plume convection, are remarkably similar to those experimented in a three-dimensional tank.

These studies were conducted in a Hele-Shaw cell, 15 cm wide × 22 cm tall × 0.1 cm thick. In order to be able to make comparisons with our previous experimental results

(Chen & Chen 1991), this set of experiments was also done with a 26% NH_4Cl–H_2O solution. In preliminary experiments, we obtained the growth rate of the mush when the temperature of the bottom was set at -21 °C (Chen 1992). In 110 min, the mush attained a height of 2 cm. In an experiment conducted in a three-dimensional tank with a high bottom temperature, $T_B = -9.5$ °C, the mush attained the same height in less than 60 min (Chen & Chen 1991). The difference can be attributed to the slower rate of transport of the warm and richer fluid to the interface where solidification takes place. We also found that, in order to sustain the plume convection to fully developed stages, T_B must be -21 °C or less; results reported here are for $T_B = -21$ °C. This is due to the slower freezing rate encountered in the Hele-Shaw cell.

Copley *et al.* (1970) reported that, in the beginning of the solidification process, crystals broken off from the dendrite tips could be seen being carried along by the convection current. It was a surprise to us that the same phenomenon occurred in the Hele-Shaw experiment where the flow is so much less vigorous. In a photo taken at $t = 0{:}15$, figure 3(a), a number of tiny crystals can be seen to move upward with the convection current. The camera was equipped with a close-up lens and an extension ring so as to achieve a 1:1 picture ratio. This means that the photos show an area 35 mm × 24 mm in the test tank. All photos were taken at f8 and 1/15 s exposure. By projecting the slide on a screen and measuring the streak marks made by these crystals, we obtained a velocity range between 1.5 and 2.5 mm s^{-1}.

In a series of six photos taken in a 50 min period, we illustrate the onset and eventual demise of a chimney. At $t = 0{:}50$, the mushy layer had grown to a height of approximately 1.4 cm. The camera was focused on two likely sites of chimneys, as shown in figure 3(*b*). In figure 3(*c*), taken 15 min later, a passage was being cleared by melting in the one on the right, creating a fully developed chimney, whereas the one on the left was being filled by dendrites. At $t = 1{:}15$, figure 3(*d*), the upper two-thirds of the chimney was completely cleared. Subsequently, the flow within the chimney became weaker and solidification took place at its exit, shown in figure 3(*e*) at $t = 1{:}20$. The entire chimney was slowly being filled by dendritic growth, as shown in figure 3(*f*) at $t = 1{:}30$ and in figure 3(*g*) at $t = 1{:}40$. The propagation of the chimney downward from the liquid–mush interface can be explained as follows (Tait & Jaupart 1992*b*): As the mushy layer becomes unstable, convective motion onsets that consists of upwelling and downwelling currents. Local equilibrium requires dissolution along upwelling and crystallization along downwelling. Assuming that the dissolution rate is constant throughout the depth, the chimney opening will first appear at the interface, where the solid fraction is approaching zero. Then, it propagates downward as the solid fraction increases toward the bottom.

In figure 3(*h*), we show a fully developed chimney near the right end wall of the cell at $t = 2{:}00$. There is a large root system near the bottom feeding the chimney with the depleted solution. After a long clear passage has been created by dissolution in the chimney (figure 3*d*–*h*), small crystals created by melting can be seen in the channel. Tiny pieces are being carried upward by the flow, and larger pieces are sinking downward, piling up at the bottom. This may explain the presence of the root system usually found at the bottom of chimneys. Some of the crystals near the wall are caught by the dendrites there. By scaling with the width of the photo (35 mm), the chimney width was determined to be between 0.1 and 0.14 cm.

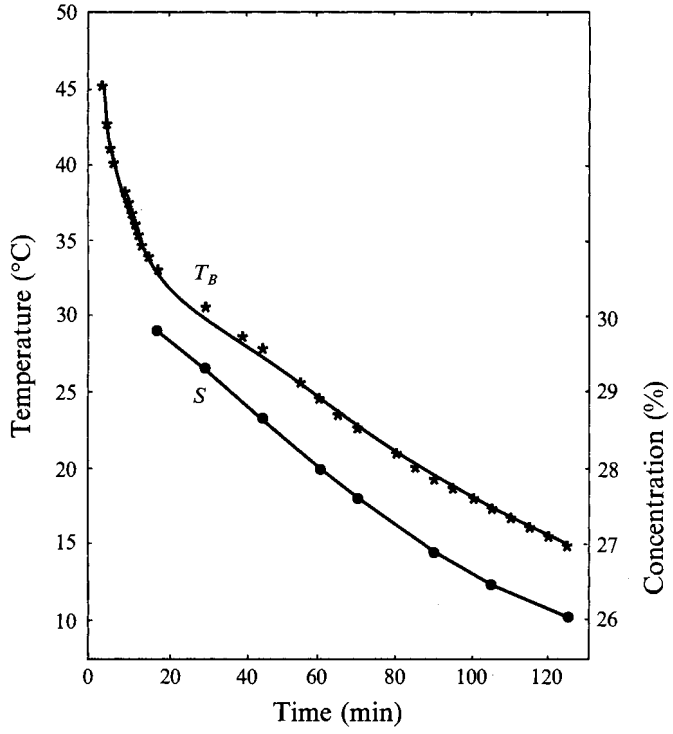

FIGURE 4. Variation of temperature, T_B, at the interior bottom wall of an all-Plexiglas tank containing 30% NH_4Cl–H_2O solution being cooled from below. Crystallization in the centre of the tank started at $t = 17$ min into the experiment. The liquidus concentration, S, corresponding to T_B is also shown for $t \geqslant 17$ min.

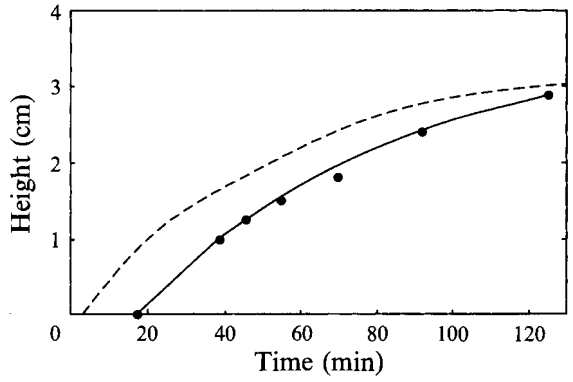

FIGURE 5. Growth of the mush in the all-Plexiglas tank (——) compared with that obtained in a tank with a copper bottom (– – –).

4. X-ray tomography experiments

We have shown (Chen & Chen 1991) that it is possible to determine the solid fraction of a mushy layer by means of X-ray tomography. Since then, the technique has been improved, enabling us to determine both the temporal and spatial variations of the solid fraction in a three-dimensional slab of a growing mushy layer.

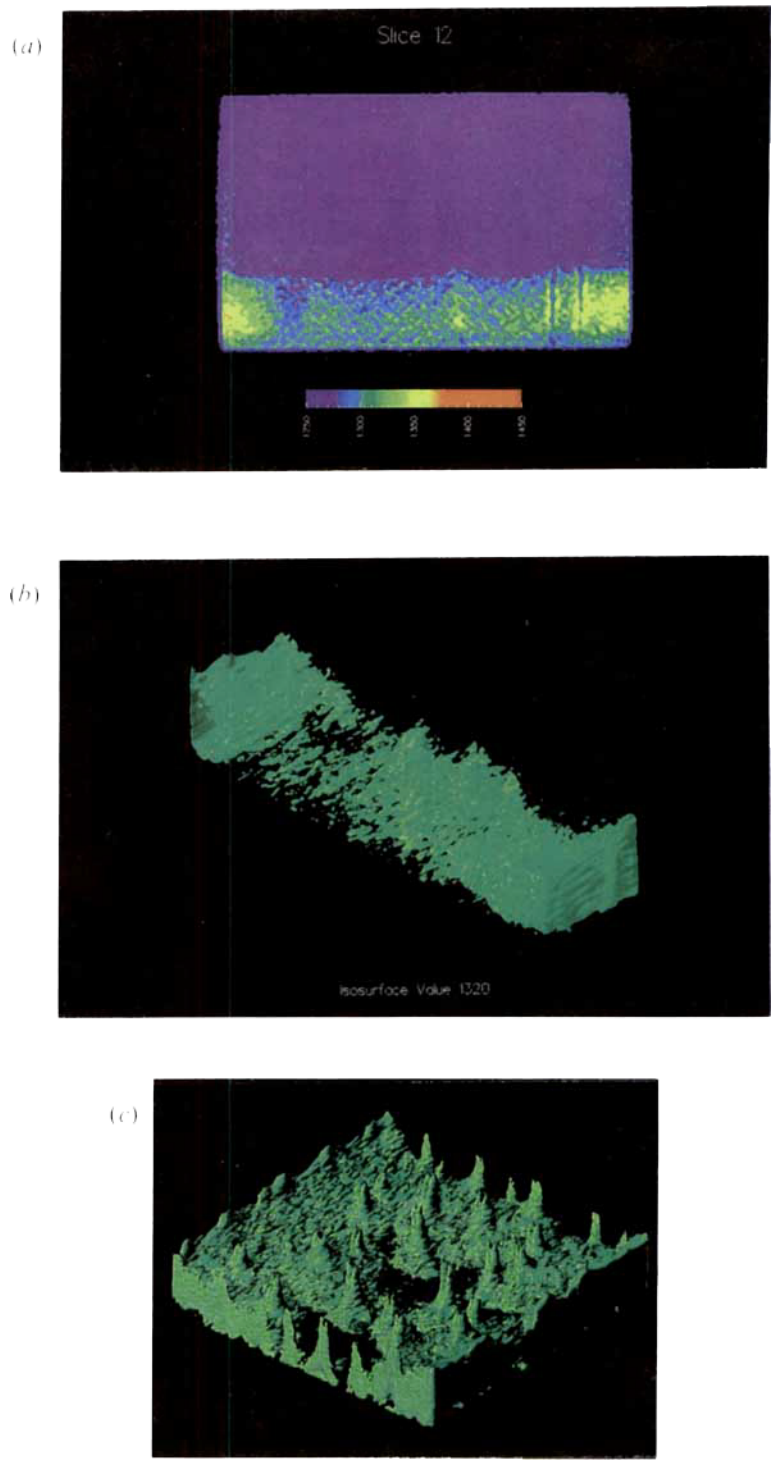

FIGURE 6. (*a*) A false-colour plot of the X-ray scan values obtained for slice 12 during the last set of scans $t = 1:33$). Blue (1250) and red (1450) correspond approximately to 0 % and 45 % solid fraction, respectively. The walls surrounding the two chimneys at the right side show higher solid fractions. Contrary to intuition, the solid fraction of the mush at the bottom, where the temperature is lowest, is generally lower than that in the middle of the mush. (*b*) A three-dimensional isosurface constructed

4.1. *Experimental procedure*

In order to avoid any spurious reflections and refractions of the X-rays, the test apparatus was made with no metallic parts. The test tank, a cube with a linear dimension of 13 cm, and the heat transfer plate were made of Plexiglas and nylon screws. Because of the low heat conductivity of the Plexiglas, the concentration of the NH_4Cl solution was increased to 30% so that a mushy layer of reasonable thickness (~ 2 cm) could be solidified in a reasonable amount of time (~ 2 h). A preliminary experiment was conducted to characterize the solidification process in this new apparatus. The initial temperature of the solution was raised to 55 °C to ease the dissolution of the NH_4Cl crystals. The coolant in the constant-temperature bath was pre-cooled to -35 °C. At the start of the experiment, $t = 0$, the tank was covered with a Plexiglas lid to prevent excessive evaporation and the coolant was pumped through the passages provided in the heat transfer plate upon which the test tank was set. Temperatures at the interior bottom wall of the tank, T_B, were recorded and are shown in figure 4. The temperature decreased sharply to 33.1 °C at $t = 0{:}17$, when crystals started to form at the bottom wall in the centre of the tank. The corresponding equilibrium concentration of the solution, S, was 29.8%, indicating approximately 1 °C undercooling, consistent with the experimental results of Worster & Kerr (1994). Such equilibrium concentrations evaluated at selected times are also shown in figure 4. From $t = 0{:}17$ on, owing to the heat release of solidification, the rate of temperature decrease became smaller and remained almost constant at approximately -0.17 °C min^{-1} to the end of the experiment at $t = 2{:}05$. This cooling rate is much smaller than that obtained in our earlier work in which both the bottom of the test tank and the heat transfer plate were made of brass. Typically, the final constant bottom temperature was reached in 20 min in the earlier experiments (Chen & Chen 1991). The equilibrium concentration of the solution corresponding to T_B decreased to 26%. The temperature of the exterior bottom wall decreased from 4.2 °C at $t = 0{:}03$ to -17.0 °C at the end of the experiment. No eutectic layer was formed throughout the experiment. The growth of the mushy layer is shown in figure 5. The final height attained by the mushy layer was 2.9 cm at $t = 2{:}05$. The growth of the mush as obtained in our previous work is sketched in the figure with a dashed line. The onset of crystallization was much earlier. But at later times, the growth rate in these two different experiments approach each other.

The same test conditions were duplicated as closely as possible for the scanning experiment carried out in a Siemens Somatom DRH CT Scanner at the Arizona Health Sciences Center. It is noted that, during scanning, only the heat transfer plate was insulated at the bottom and the sides with 2 cm thick Styrofoam. The test tank was not insulated to facilitate visual observation from the control room during scanning. The preliminary test was made under the same conditions and, except for some descending plumes due to evaporation at the start of the experiment, no spurious convection along the sidewall was observed in the shadowgraph. Scanning was started at $t = 0{:}32$, when the mush was approximately 1 cm thick. The thickness of the vertical sheet of X-rays was 2 mm. After each scan, the table was advanced 2 mm for the next scan. This procedure was repeated for 15 scans, covering a total width of 3 cm in the

---

from the data of 15 slices during the last set of scans at $t = 1{:}27$–$1{:}34$, with a 7 min time delay between the front and back slices. Within the green space, $\phi \geqslant 0.167$. The solid fraction of the mush near the bottom is generally lower throughout the entire slab. (*c*) The well-developed chimneys in an earlier solidification experiment are clearly exhibited in this isosurface plot. Within the green space, $\phi \geqslant 0.346$. The colour scale for this plot is different from that for (*a*) and (*b*).

middle of the tank. The time required for the 15 scans was approximately 7 min. The table was then returned to the original position, ready for the next set of scans. The second set was started 15 min after the start of the first set. Subsequently, sets of scans were spaced at 10 min intervals.

4.2. *Results and discussion*

The data for slice 12 of the last set of scans, $t = 1{:}33$, are shown in false colours in figure 6(*a*). The scan value scale, from 1250 to 1450, can be calibrated to yield the Hounsfield unit or the CT number (Barrett 1981), which is the X-ray attenuation coefficient, μ, normalized with respect to that of water. By assuming that the X-ray attenuation coefficient of the mush, μ, can be expressed as

$$\mu = \phi\mu_s + (1-\phi)\mu_f,$$

in which ϕ is the solid fraction and the subscripts s and f denote solid and fluid, respectively, the solid fraction can be calculated once μ is measured since μ_f and μ_s are known. The colours blue (1250) and red (1450) correspond to approximately 0% and 45% solid fraction, respectively. Two chimneys are clearly visible on the right side of the tank, with high solid fraction along the chimney wall. It can be discerned, upon close examination, that there is a horizontal layer slightly above the bottom whose scan value is lower (mostly blue) than that of the layer next to the bottom (mostly green and yellow). This is discussed and quantitatively displayed later in figures 8 and 9.

By combining all 15 scans, a three-dimensional isosurface can be constructed. Such a surface for the scan value of 1320, corresponding to a solid fraction of 0.167, is shown in figure 6(*b*). Note that there is a time delay of 7 min between the front and the back slices. The solid fraction is generally higher near the two sidewalls, where additional cooling was effected by heat conduction through the Plexiglas. This isosurface plot clearly exhibits that the solid fraction of the mush is quite variable within the layer, and it is generally lower near the bottom wall all across the slab.

In an earlier experiment, 30% NH_4Cl solution was directionally solidified in the same Plexiglas tank, but with a brass heat transfer plate at the bottom. Cooling was stopped at 1 hr 40 min, when there were a number of well-developed chimneys in the mush. X-ray tomography was performed 2 h after the end of the experiment. A series of three-dimensional contour plots at increasingly larger solid fractions were constructed from the data. In figure 6(*c*) we show the isosurface for $\phi = 0.346$. Regions of solid fraction $\geqslant 0.346$ are coloured green (note that the colour scale for figure 6*c* is different from that for figures 6*a* and 6*b*). The increase in solid fraction of the mush in the neighbourhood of the chimneys and their root systems is dramatically displayed.

The solid fraction distribution in the mush surrounding the two chimneys shown in figure 6(*a*) is shown by a contour map in figure 7. We selected a region 50 scan lines wide (x) by 60 scan lines high (z), corresponding to a physical area of 2.23 cm × 2.68 cm. The solid fraction values shown are the results of smoothing by taking the average of a 3×3 matrix of pixels surrounding each point. The x-axis is arbitrary, while the z-axis starts at the bottom of the tank. In data reduction, it is assumed that the scan value of the liquid within the mush is constant. Results show the characteristic sharp increase of solid fraction at the rim of each chimney and the general decrease of solid fraction ϕ toward the mush–liquid interface. Note, however, that the peaks of solid fraction do not occur at the bottom of the tank. After attaining the maximum values, solid fraction decreases toward the bottom, as indicated in figure 6(*a*). The chosen height of 2.68 cm is slightly larger than the thickness of the mush. This explains the fact that some contours near the top show negative value of ϕ. In reality, they indicate the local

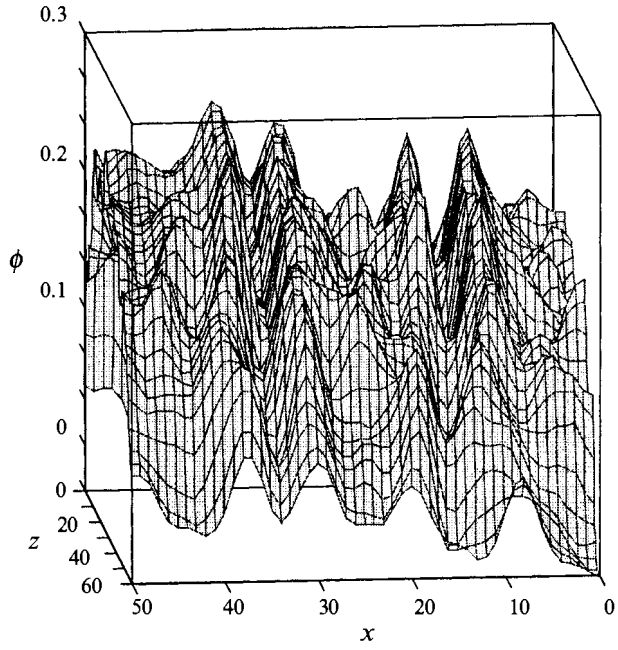

FIGURE 7. Solid fraction distribution in the neighbourhood of the two chimneys shown in figure 6(*a*). The horizontal distance (x) is 50 scan lines (2.23 cm) and the vertical distance (z) is 60 scan lines (2.68 cm), with $z = 0$ at the bottom. Data are smoothed by taking the average of the solid fraction value in the 3×3 matrix of pixels surrounding each point. The large increase in solid fraction at the rims of the chimneys is clearly exhibited.

variations of NH_4Cl concentration in the solution. It is interesting to compare our measured results with those obtained by Amberg & Homsey (1993). They computed the solid fraction distribution in the neighbourhood of a chimney for the physical parameters $\delta = 0.3$, $C_s = 1$, and $S_t = 1$, where δ is the Péclet number, or the non-dimensional thickness of the mush; C_s is a modified concentration ratio; and S_t is the Stefan number:

$$\delta = \frac{\mathrm{d}V}{\kappa}, \quad C_s = \delta\left[\frac{c_s - c_0}{c_0 - c_B}\right], \quad S_t = \frac{L}{C_p[T(c_0) - T_B]},$$

where d is the mush thickness; V is the freezing velocity; κ is the thermal diffusivity; c_s, c_0, and c_B are the concentrations of the solid phase, the initial solution, and the equilibrium solution at the bottom temperature, T_B, respectively; L is the latent heat; C_p is the specific heat of the fluid, and $T(c_0)$ is the liquidus temperature corresponding to c_0. The results are shown in a contour map presented in figure 4 of their paper. The set of parameters δ, C_s, S_t for our experiment was 0.6, 5 and 5, respectively. In spite of these differences, the magnitudes of solid fractions are comparable and the general characteristics are quite similar, with the exception of the root system at the bottom of the chimney.

Horizontally averaged values of scanned data in the central 9 cm region for slice 12 at all six scan times are shown in figure 8(*a*). Regions near the sidewalls with abnormally high solid fractions are excluded, but the inner chimney on the right and the low-solid-fraction region (blue, cf. figure 6*a*) are included in the averaging. Results are shown from 2 cm below the free surface to the bottom of the tank. Some spurious readings near the free surface, possibly due to reflection and refraction effects, are thus

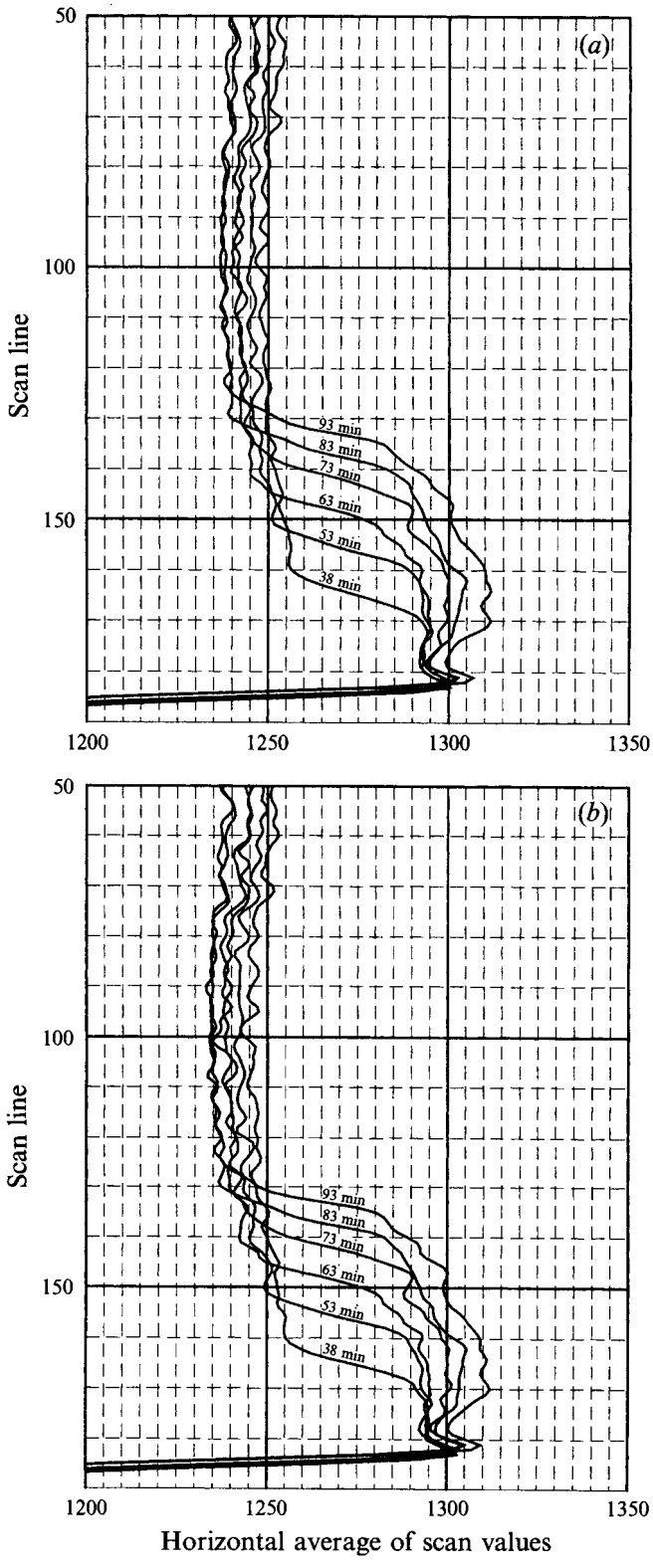

FIGURE 8. For caption see facing page.

excluded. The bottom of the tank is located at the sharp peak of the scan value. Below this point, the scan value decreases precipitously because Plexiglas is quite transparent to X-rays. In the liquid region, the average scan value becomes smaller with time because the NH_4Cl concentration is decreasing due to the crystallization process. These curves show the growth of the mush in thickness, as well as in solid fraction, as time progresses. One curious fact is the significant decrease in the scan value near the bottom at the three later times. This was thought to be due to the effect of the large root system occurring at the bottom of the chimney and of the region of low scan value on the left. Another averaging was made of a smaller central region of 6.4 cm excluding both of these features (figure 8*b*). The results are almost the same as those shown in figure 8(*a*). The decrease in scan value near the bottom, though slightly smaller, is still prominently displayed.

The scan values are then converted into solid fractions, ϕ, and the scan lines are converted into height from the bottom using the data from figures 8(*a*) and 8(*b*). The results are shown in figures 9(*a*) and 9(*b*), respectively. In data reduction, to obtain more precise values of ϕ, the decrease in scan value of the liquid due to the decrease in concentration from the top to the bottom of the mush was accounted for. The scan value of the liquid at the top of the mush is obtained from figures 8(*a*) and 8(*b*). The liquid at the bottom of the mush is assumed to be at the liquidus concentration corresponding to the temperature there (as shown in figure 4). A linear variation of the scan value through the mush is assumed. It is seen that the general features of the two curves shown in figures 9(*a*) and 9(*b*) are quite similar. The height indicated by $\phi = 0$ is the location of the liquid–mush interface at the highest point of the mushy layer (see figure 6*a*). The average thickness of the mushy layer, defined to be the mean height of the region of rapidly increasing ϕ and obtained from either figure 9(*a*) or 9(*b*), shows good agreement with the results of the preliminary experiment (figure 5). In the bulk of the mush, solid fraction is nearly uniform at early times. This may be explained by the small temperature difference across the mushy layer. As time progresses, the temperature difference increases, causing a larger variation of solid fraction from the top to the bottom of the layer. At later times, $t \geqslant 1{:}13$, when the chimneys are well established, there is a substantial decrease in the solid fraction as the bottom is approached. The decrease is only slightly larger when the chimney is included in the averaging (figure 9*a*) than when it is not (figure 9*b*).

Data shown in figure 8(*b*) indicate that the time rate of increase of the solid fraction, $\partial\phi/\partial t$, is approximately constant in the mush up to $t = 1{:}13$. Beyond this time, when the chimneys are becoming well developed, $\partial\phi/\partial t$ in the bottom 3–4 mm of the mush becomes much less than that in the rest of the mush. The mechanism for such an occurrence is not clear at present. But the consequence is quite clear. The permeability of the mush near the bottom is increased up to 50%, providing a passage for the liquid flow toward the chimneys.

The average solid fractions in the bulk of the mush are 0.083, 0.100 and 0.137 at $t = 0{:}38$, 1:03, and 1:33, respectively. These values are in good agreement with those obtained by a mass balance in the tank. Using a value of 0.1 for the average solid fraction of the mushy layer just prior to the onset of plume convection, our estimate of the critical Rayleigh number is within a factor of 1.6 of the value found by Tait & Jaupart (1992*a*). These critical Rayleigh numbers are in general agreement with the

FIGURE 8. Horizontally averaged scan values in the central portion of the tank for slice 12 at $t = 0{:}38$, 0:53, 1:03, 1:13, 1:23 and 1:33: (*a*) central 9 cm region including the inner chimney on the right; (*b*) central 6.4 cm region excluding the chimney. The mush is growing in thickness and solid fraction while the concentration of the melt is decreasing.

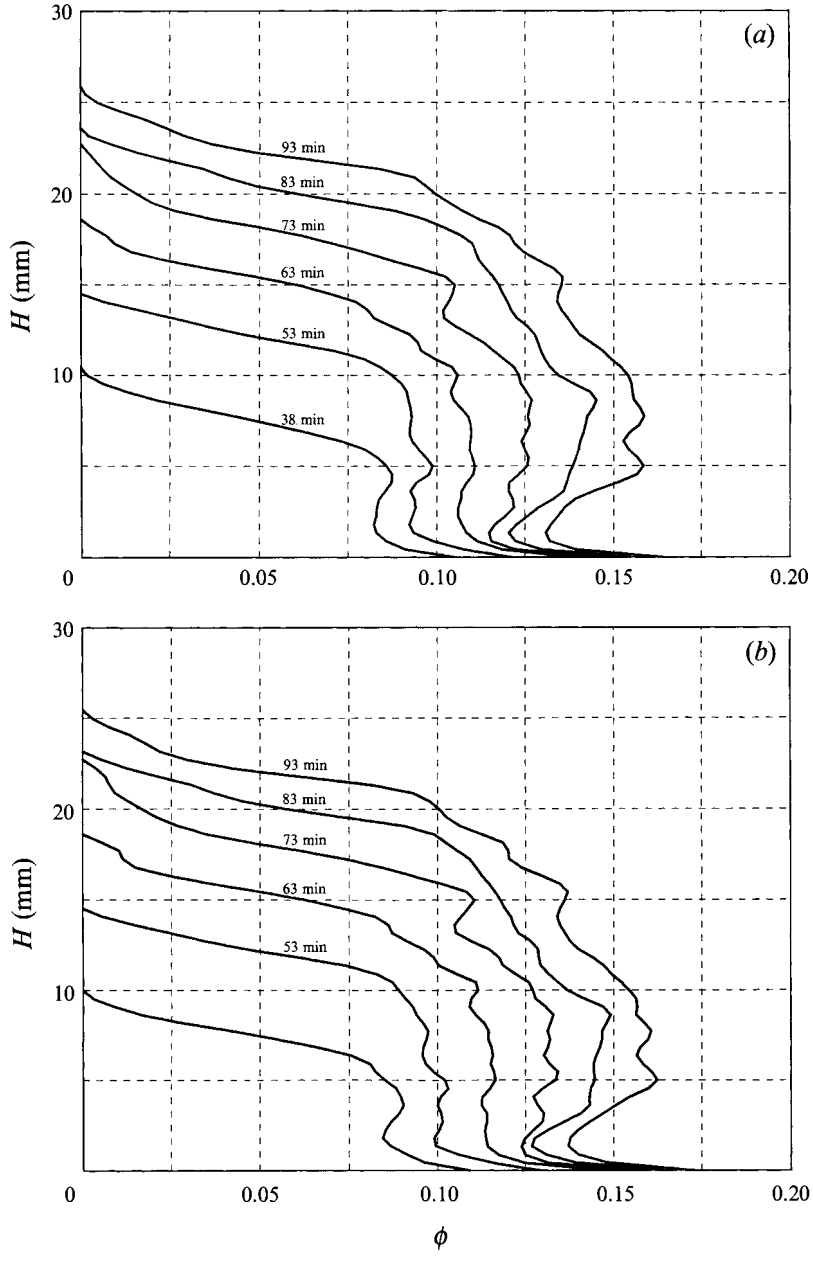

FIGURE 9*a*, *b*. Horizontally averaged solid fraction values in the mush for slice 12 corresponding to the data shown in figures 8(*a*) and 8(*b*), respectively. At $t = 1{:}33$, the sharp decrease of the solid fraction near the bottom causes an increase of the local permeability of the much by approximately 50%.

predictions of Worster (1992). If $\phi = 0.1$ is used in the equation recommended by Chen *et al.* (1994), the resulting critical Rayleigh number is also in general agreement with those cited above.

5. Conclusions

From the results reported herein and those of earlier investigators, the sequence of significant events in a growing mush generated by directional solidification is as follows. In the early stages of development of a mushy layer, crystallization occurs mainly at the top of the mush, releasing low-concentration liquid, which rises through a number of finger cells. The liquid within the mush is quiescent, and crystallization proceeds at a rate sufficient to maintain equilibrium conditions as the temperature slowly decreases. The Rayleigh number of the layer increases as both the thickness and the concentration difference across the layer increase. The formation of chimneys, with associated plume convection, onsets when the Rayleigh number exceeds its critical value. Finite-amplitude perturbations in the liquid, such as those created by suction near the mush–liquid interface, cannot promote the onset of chimneys when the cooling is effected by a constant-temperature bath. The upward plume flow in the chimneys induces a downward flow into the mush, thus reducing the upward flow of the finger convection. As the chimney develops, the solid fraction around the rim of the chimney increases. However, through a mechanism not understood at present, the solid fraction at the bottom of the mushy layer remains low. As a consequence, the flow in the chimney is maintained by drawing liquid downward through the mush, then in horizontal streams along the bottom. It is hoped that some of the results reported here will encourage further research on this complex phenomenon.

The experiments on dye tracing and on the structure of the mush layer in a Hele-Shaw cell were performed in the GFD Laboratory of the Research School of Earth Sciences, Australian National University, during the summer of 1991. I thank Professor Stewart Turner for his kind hospitality and Messrs Beasley, Wylde-Brown, and Corrigan for their able assistance. I thank Dr Evan Unger, Director of MRI/CT at the Arizona Health Sciences Center, for his cooperation and Ms Nicky Bertolleti for performing the scans. Marvin Landis of the Center for Computing and Information Technology, The University of Arizona, processed the CT data into three-dimensional images and other graphical information. His help is greatly appreciated. Financial support provided by the NASA Microgravity Science and Application Division through Grant NAG 3-1268 is gratefully acknowledged. Finally, I wish to thank the referees for their thoughtful and constructive comments.

REFERENCES

AMBERG, G. & HOMSY, G. M. 1993 Nonlinear analysis of buoyant convection in binary solidification with application to channel formation. *J. Fluid Mech.* **252**, 79–98.

BARRETT, H. H. 1981 *Radiological Imaging*, pp. 334, 376. Academic.

CHEN, C. F. 1992 Convection in the mushy zone during directional solidification. In *Interactive Dynamics of Convection and Solidification* (ed. S. H. Davis, H. E. Huppert, U. Müller & M. G. Worster), pp. 139–141. Kluwer.

CHEN, C. F. & CHEN, F. 1991 Experimental study of directional solidification of aqueous ammonium chloride solution. *J. Fluid Mech.* **227**, 567–586.

CHEN, F., LU, J. W. & YANG, T. L. 1994 Convection in directional solidification of aqueous ammonium chloride solutions. *J. Fluid Mech.* **276**, 163–188.

COPLEY, S. M., GIAMEI, A. F., JOHNSON, S. M. & HORNBECKER, M. F. 1970 The origin of freckles in unidirectionally solidified castings. *Metall. Trans.* **1**, 2193–2204.

EMMS, P. W. & FOWLER, A. C. 1994 Compositional convection in the solidification of binary alloys. *J. Fluid Mech.* **262**, 111–139.

HELLAWELL, A. 1987 Local convective flows in partly solidified alloys. In *Structure and Dynamics of Partially Solidified Systems* (ed. D. E. Loper). NATO Series E, Vol. 125, pp. 3–22. Martinus Nijhoff.

HELLAWELL, A., SERAZIN, J. R. & STEUBE, R. S. 1993 Channel convection in partially solidified systems. *Phil. Trans. Roy. Soc. Lond.* A **345**, 507–544.

MCDONALD, R. J. & HUNT, J. D. 1970 Convective fluid motion within the interdendritic liquid of a casting. *Metall. Trans.* **1**, 1787–1788.

ROBERTS, P. H. & LOPER, D. E. 1983 Towards a theory of the structure and evolution of a dendritic layer. In *Stellar and Planetary Magnetics* (ed. A. M. Soward), pp. 329–349. Gordon and Breach.

SAMPLE, A. K. & HELLAWELL, A. 1984 The mechanisms of formation and prevention of channel segregation during alloy solidification. *Metall. Trans.* A **15**, 2163–2173.

SARAZIN, J. R. & HELLAWELL, A. 1988 Channel formation in Pb–Sn, Pb–Sb, and Pb–Sn–Sb alloy ingots and comparison with the system NH_4Cl-H_2O. *Metall. Trans.* A **19**, 1861–1871.

TAIT, S., JAHRLING, K. & JAUPART, C. 1992 The planform of compositional convection and chimney formation in a mushy layer. *Nature* **356**, 406–408.

TAIT, S. & JAUPART, C. 1992*a* Compositional convection in a reactive crystalline mush and melt differentiation. *J. Geophys. Res.* **97**, 6735–6756.

TAIT, S. & JAUPART, C. 1992 New experiments on compositional convection. In *Interactive Dynamics of Convection and Solidification* (ed. S. H. Davis, H. E. Huppert, U. Müller & M. G. Worster), pp. 155–158. Kluwer.

WORSTER, M. G. 1991 Natural convection in a mushy layer. *J. Fluid Mech.* **167**, 481–501.

WORSTER, M. G. 1992 Instabilities of the liquid and mushy regions during directional solidification of alloys. *J. Fluid Mech.* **237**, 649–669.

WORSTER, M. G. & KERR, R. C. 1994 The transient behaviour of alloys solidified from below prior to the formation of chimneys. *J. Fluid Mech.* **269**, 22–44.